

Solvated Membrane Nanodiscoids: A Probe For The Effects Of Gaussian Curvature

R. G. Morris^{1,2,3}, T. R. Dafforn⁴ and M. S. Turner¹

¹*Department of Physics and Centre for Complexity Science,
University of Warwick, Coventry CV4 7AL, UK*

²*Simons Centre for the Study of Living Machines,
National Centre for Biological Sciences, TIFR, Bangalore, 560064, India*

³*EMBL-Australia, University of New South Wales, Sydney, Australia and*

⁴*School of Biosciences, University of Birmingham, Birmingham, B15 2TT, UK*

(Dated: January 7, 2022)

Several methods now exist to solvate lipid bilayer discoids at the scale of tens of nanometres. Due to their size, such nanodiscoids have a comparatively large boundary-to-area ratio, making them unusually well-suited to probing the effects of Gaussian curvature. Arguing that fluctuations in discoid size and shape are quenched on formation, we quantify the stability, in terms of size and shape, of near-solvation discoid-like flaps that are subject to thermal fluctuations. Using cryo-Electron Microscopy images of Styrene Maleic Acid stabilised discoids, we deduce that stable, saddle-like discoids (with high Gaussian curvature) can likely be solvated from bulk lamellar (L_α) phase at moderate-to-high surface tensions ($> 10^{-4}$ N/m). We then describe how such tension-controlled solvation can be used for both measuring, and fractionating membrane components according-to, the modulus of Gaussian rigidity $\bar{\kappa}$. Opportunities for investigating the effects of Gaussian curvature on membrane-embedded proteins, which can be co-solvated during the formation process, are also discussed.

I. INTRODUCTION

Several long-chain molecules have now been shown to solvate nanoscale lipid bilayer discoids, with two prominent examples being the copolymer Styrene Maleic Acid (SMA) [1–4] and the α -helical lipoprotein APO-A1 [5–7]. The key feature of these molecules is their amphipathic structure: in the presence of a lipid bilayer, the hydrophobic groups interact with the acyl chains of the lipids, whilst the hydrophilic parts face the solvent, resulting in a solution of stable nanodiscoids (see Fig. 1). Significantly, such discoids have been shown to preserve the integrity of co-solvated transmembrane proteins, implying an important role for the purification, structural determination, and functional characterization of membrane proteins [7–14].

The modulus of Gaussian rigidity, $\bar{\kappa}$, quantifies a membrane's preference for forming locally saddle-like or spherical shapes, and determines the equilibrium topology of bulk membrane phases, *e.g.*, a highly connected sponge (L_3), one or more (large) membranes (L_α) or a large number of small vesicles [15]. However, $\bar{\kappa}$ is notoriously difficult to measure. This is because of the Gauss-Bonnet theorem [15–17], which states that Gaussian curvature doesn't couple to any observable deformation modes for one component membranes of fixed, boundary-free topology. Even for membranes with a boundary (or a hole [18]), the coupling to Gaussian curvature is usually negligible for all but the largest boundary-to-area ratios. Solvated nanodiscoids have an extremely large boundary-to-area ratio, making them not only technologically important, but also uniquely suited for studying the role of $\bar{\kappa}$ in membranes.

In this article we study how lipid nanodiscoids can be used to probe phenomena that couple to Gaussian curva-

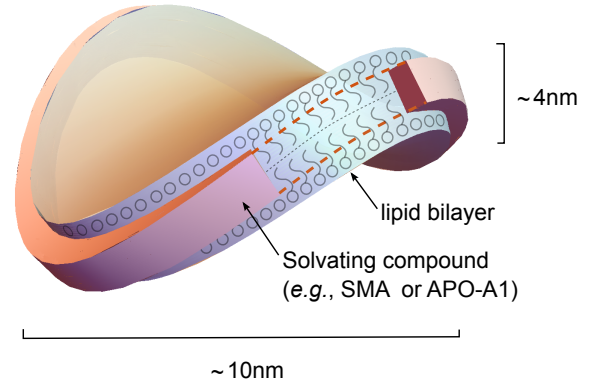


FIG. 1. (Colour online) Sketch of a saddle-shaped nanoscale lipid bilayer discoid. The structure is stabilised by the amphipathic nature of the solvating compound (*e.g.* SMA or APO-A1): the hydrophobic groups interact with the acyl chains of the lipids, whilst the hydrophilic groups face the solvent. The large boundary-to-area ratio of these structures makes them ideally suited for probing phenomena that couple to Gaussian curvature.

ture. We show how they can be used to both indirectly measure $\bar{\kappa}$, and fractionate lipids by $\bar{\kappa}$ into discoids with negative Gaussian curvature. More generally, given the extreme values of Gaussian curvature, both positive and negative, found in vesicles and organelles associated with protein synthesis and sorting [19, 20], it is natural to ask: what are the effects of this curvature on membrane-embedded proteins, and does it play a role in sorting. In this context, lipid nanodiscoids may have a wider role as a tool for investigating the effects of Gaussian curvature on co-solvated transmembrane proteins.

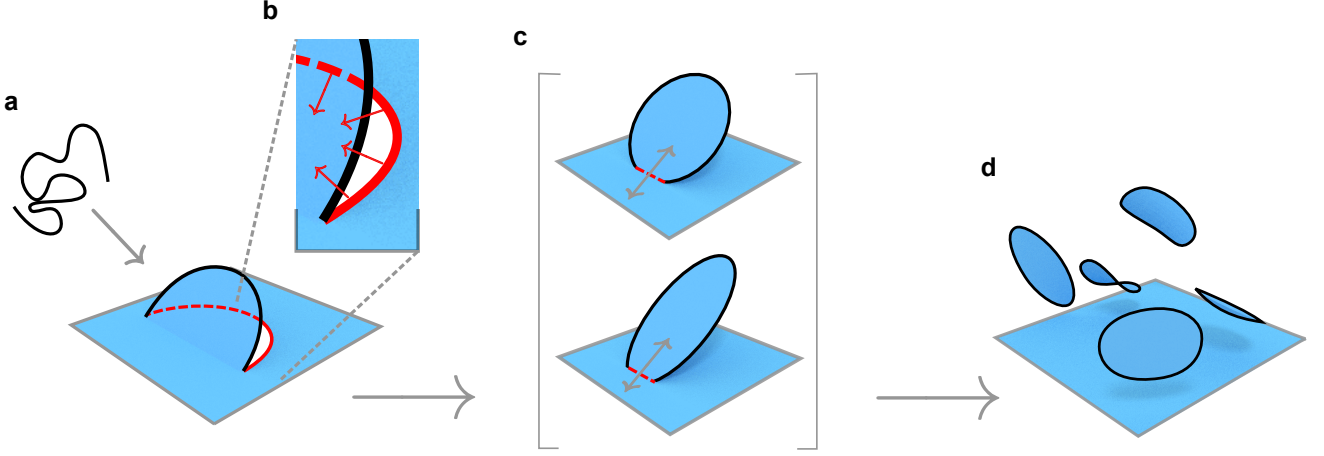


FIG. 2. (Color online) Cartoon of the putative formation process. Driven by its amphiphilic character, the solvating long-chain molecule inserts into the membrane (a). The presence of the solvating compound leads to a hole and a free edge (red dashed line) in the membrane. The high energetic cost of such free edges, however, drives the closure of such holes, first forming a straight ‘cut’ and then bringing the two ends of the solvating molecule together (b). Near solvation, a small membrane flap remains (b and c) which can still exchange molecules with the bulk membrane. On ‘pinching-off’, the differences in flap size and shape that result from such fluctuations become quenched, since the elastic modulus of membranes held at fixed particle number is extremely large. The result is a polydisperse mixture of solvated nanodiscoids (d).

II. POLYDISPERSITY QUENCHED ON FORMATION

We begin with the observation that solvated nano-scale discoids form a relatively polydisperse mixture, with an apparently broad range of areas and shapes. Since lipid bilayers are essentially incompressible, we conclude that such variation is a result of the formation process, which is poorly understood. Moreover, we note that the timescales of dissipation, due to either the viscosity of the bilayer, or the surrounding water, are comparatively short. We therefore assume a quasi-static description of nanodisc solvation, which we use to quantify the statistics of area and shape variation, and hence imply the aforementioned new role for nanodiscoids in the context of the probing of Gaussian curvature.

Neglecting any potential complications associated with adsorption/insertion, our starting point is a fully-inserted protein/co-polymer restricted to planar self-avoiding conformations (*i.e.*, crossings are not allowed). It is assumed that the (known) amphipathic properties of the long-chain solvating molecule then lead the formation of a flap of bilayer, able to protrude discontinuously from the membrane (see Fig. 2). The large energy-per-unit-length associated with an unadorned bilayer edge then ensures that the “hole” left behind by such a flap quickly becomes a “cut”, which effectively runs in a straight line between the two ends of the solvating protein/co-polymer (see red and red-dotted lines in panels a, b and c of Fig. 2). Further energy minimization then drives the meeting of the two free ends, reducing the cut length, and leading to discoid solvation. Very close to formation, when the cut is very small, an effective line tension can be associated

with the closed curve comprising the boundary of the near-solvation flap and the cut itself.

Provided that it is very near the point of “closure” (when the protein/co-polymer ends meet) and that it retains the structure (and symmetry) of a standard bilayer, a Helfrich-like continuum theory [16] can be used for the bulk of the flap. Assuming uniform lipid composition, the leading order energetics [21] are related to the geometry of the midsurface \mathcal{S} of the discoid-like flap via

$$\mathcal{H}_m = \int_{\mathcal{S}} dA \left[\sigma + \frac{\kappa}{2} (2H - c_0)^2 + \bar{\kappa} K \right], \quad (1)$$

where σ is a surface tension, set by exchange of lipids through the almost-closed gap between protein/co-polymer ends. As usual, H and K are the mean and Gaussian curvatures, and κ is the membrane bending rigidity. We assume that there is no density mismatch between bilayer leaflets and therefore take $c_0 = 0$ throughout.

There is also an energy associated with boundary, $\partial\mathcal{S}$, which is the closed line formed by concatenating the solvating protein/co-polymer and the remaining small cut. We include both a line tension τ , and an energetic cost to bending (amphipathic asymmetry precludes any twist). By symmetry, the latter must be invariant under sign change of both the normal and geodesic curvatures of $\partial\mathcal{S}$, for which we use the symbols q_n and q_g , respectively. The contribution is written as the following line integral

$$\mathcal{H}_b = \int_{\partial\mathcal{S}} dl \left[\tau + \frac{k_g}{2} (q_g - q_0)^2 + \frac{k_n}{2} q_n^2 \right], \quad (2)$$

where k_g and k_n are effective bending moduli. The former corresponds to in-tangent-plane bending, whilst the

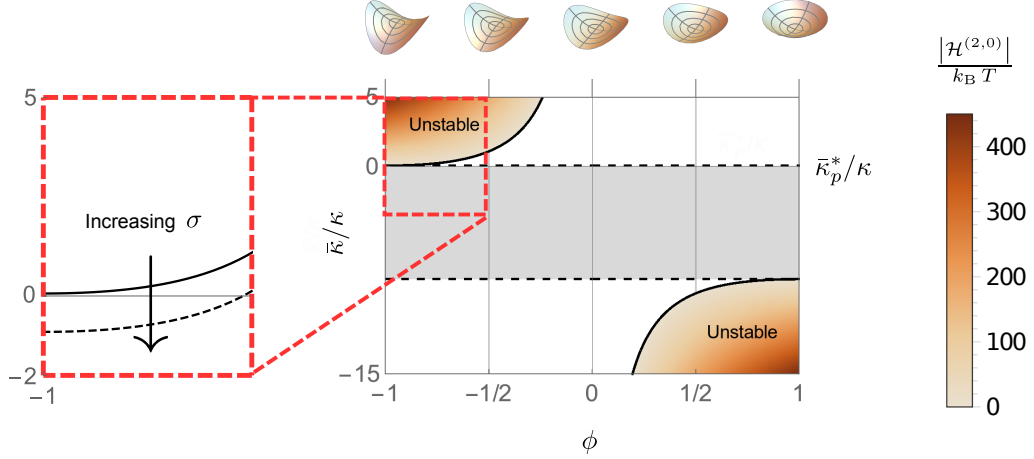


FIG. 3. (Color online) Linear stability of out-of-plane perturbations ϕ , plotted against the ratio of bending moduli $\bar{\kappa}/\kappa$, for indicative values $\kappa = 20 k_B T$, $k_g = k_n = R_0^3 \sigma$, $R_0 = 5$ nm, $\sigma = 10^{-4}$ N m $^{-1}$, and $q_0 = 1/R_0$. Regions of stability/instability are delimited by solid black lines, which correspond to the quantity $\kappa^*(\phi)/\kappa$ (see SM). Within a band of values, all perturbations are suppressed and only flat discs are stable (grey shaded region). Outside of this band, a range of shapes are unstable, with pringles (saddles with principal curvatures of equal magnitude) or shallow spherical caps being dominant when $\bar{\kappa}/\kappa$ is above or below the stable region, respectively (see ‘heatmap’ shading, which quantifies the growth rate of a given perturbation). The critical value $\bar{\kappa}_p^* = \bar{\kappa}^*(\phi = -1)$ therefore controls the transition to pringles, which spontaneously form only if $\bar{\kappa}_p^*$ is less than or equal to the Gaussian rigidity of the bilayer in question ($\bar{\kappa} = -\kappa$ for a wide variety of lipids [22]). From Eq. (7), we see that $\bar{\kappa}_p^*$ decreases linearly with σ , indicating that with sufficient tension pringles can always be rendered unstable, irrespective of the composition of the bilayer used, and hence its modulus of Gaussian rigidity (see inset).

latter corresponds to out-of-tangent-plane bending. [For definitions of the relevant geometrical quantities, see the Supplementary Material (SM)]. Notice that since the solvating protein/co-polymer is assumed to preserve the symmetry of the bilayer on reflection about \mathcal{S} (true for both SMA and APO-A1), a non-zero spontaneous line curvature (q_0) is only permitted in the tangent plane of the surface, and not in the normal direction.

Of course, once solvated, lipid exchange with the membrane (reservoir) is no longer possible. All subsequent area and shape fluctuations are then suppressed by the disproportionately large intrinsic elastic modulus of lipid bilayers (when held at fixed particle number) and, as a result, any thermally-induced fluctuations in area due to lipid exchange when close to solvation become fixed, or “quenched”, for all time at the point when the discoid finally detaches.

III. TENSION CONTROLLED INSTABILITY TO PRINGLE SHAPES

To understand the ramifications of these ideas, consider flat shapes (*i.e.*, $H = K = q_n = 0$). In this case, the total energy, $\mathcal{H} = \mathcal{H}_b + \mathcal{H}_m$, is minimised by discs of radius R_0 , which is related to the line tension τ (and k_g ,

q_0 and σ) via

$$\tau = \frac{k_g}{2R_0^2} (1 - q_0^2 R_0^2) - R_0 \sigma, \quad (3)$$

(see SM for details). The in-plane stability can be investigated by writing an angle-dependent radius $R(\theta) = R_0 + \delta R(\theta)$ such that $\delta R(\theta) = \epsilon R_0 \sum_n \Re[A_n \exp(in\theta)]$, where \Re indicates the real part, $A_n \in \mathbb{C}$, $|A_n| \leq 1$ for all $n \in \mathbb{N}$, and $\epsilon \ll 1$ is dimensionless. The energy, \mathcal{H} , can then be expanded as a power series in terms of ϵ . Here, the mean-squared thermal amplitude of the n^{th} fluctuation mode follows by the principle of equipartition of energy (see SM) [23]

$$\epsilon^2 \langle |A_n|^2 \rangle = \frac{k_B T R_0}{\pi (n^2 - 1) [k_g (n^2 - 1) - R_0^3 \sigma]}. \quad (4)$$

The $n = 0$ mode is a dilation, and is always stable (we expect $\sigma, k_g > 0$ for all lipid discs, irrespective of whether they are cut from living cells, adsorbed bilayers or vesicles). The $n = 1$ mode corresponds to a translation where the disc remains circular to lowest order, and is of indeterminate amplitude. In general, for $n > 1$, a mode of degree n is stable if $k_g \geq R_0^3 \sigma / (n^2 - 1)$. This puts a lower bound $k_g \geq R_0^3 \sigma / 3$ on the geodesic rigidity of the attached solvating compound that is required for stable circular discs.

For non-flat discoids, we consider the subset of all out-of-plane deformations that can be parametrised by the

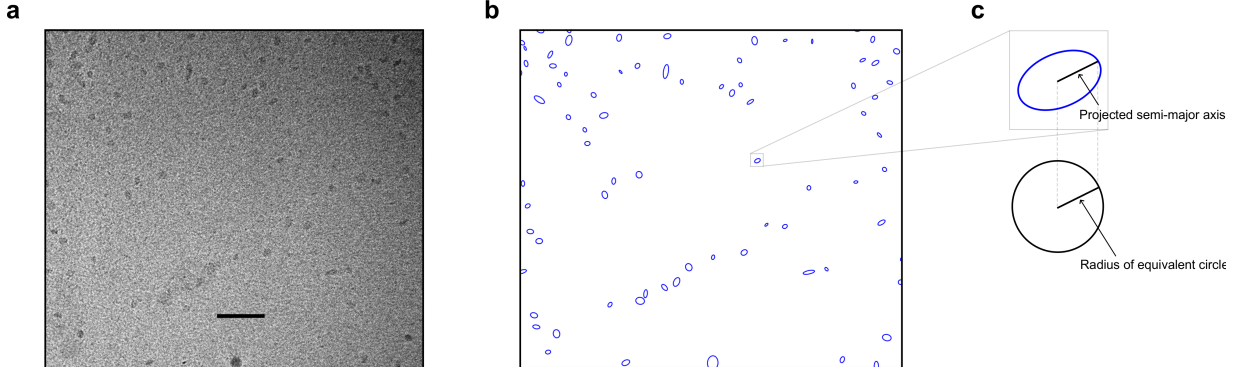


FIG. 4. (Color online). Cryo-Electron Microscopy image (a) of SMA stabilised discoids, prepared according to [4] (scale bar = 50 nm). Sufficiently large values of k_g and k_n correspond to isotropically oriented mixtures of flat discs, whose radial fluctuations are governed by Eq. (4) with $n = 0$. Therefore, using image processing tools to fit ellipsoids to each discoid (b) and extracting the mean-squared deviation of the semi-major axes (c), Eq. (4) may be used to calculate an upper estimate of $k_g \simeq 7 k_B T \text{ nm}$ and therefore an upper bound on $\sigma_p(\bar{\kappa})$, the tension above which pringles form.

two (orthogonal) principal curvatures at the centre, c_1 and c_2 . This is reasonable provided that the disc is (laterally) much smaller than the membrane correlation length $\sqrt{\kappa/\sigma}$, which is typically at least a few tens of nm. The curvatures are labelled, without loss of generality, such that $|c_1| \geq |c_2|$. Using a polar Monge approach, the height field is chosen to be

$$h(r, \theta) = \frac{\alpha r^2}{4 R_0} [1 + \phi + (1 - \phi) \cos 2\theta], \quad (5)$$

where the angle θ is measured from the direction of c_1 , $\phi = c_2/c_1$ takes values in the interval $[-1, +1]$, and $\alpha = R_0 c_1 \ll 1$ is a small dimensionless parameter. Both mean and Gaussian curvatures remain constant across the disc up to $O(\alpha^2)$ making (1) straightforward to calculate (see SM). However, this is not the case for the either line element at the boundary dl or the line curvatures q_g and q_n appearing in (2). Indeed, both dl and q_g also rely on ϵ , and we therefore adopt a notation where the $O(\alpha^a \epsilon^e)$ term in an expansion of \mathcal{H} is written as $\alpha^a \epsilon^e \mathcal{H}^{(a,e)}$. The resulting expression (see SM) has neither any first order terms [*i.e.*, at $O(\alpha)$ or $O(\epsilon)$], nor any $O(\alpha \epsilon)$ cross terms:

$$\mathcal{H} = \mathcal{H}^{(0,0)} + \epsilon^2 \mathcal{H}^{(0,2)} + \alpha^2 \mathcal{H}^{(2,0)} + O(\epsilon^3) + O(\alpha^3). \quad (6)$$

The coefficients $\mathcal{H}^{(0,0)}$ and $\mathcal{H}^{(0,2)}$ can therefore be read-off from the previously calculated energy of a flat disc [τ is unchanged from (3)]. Moreover, the earlier stability analysis holds too, but now refers to the *projected* disc size, which is independent of out-of-plane perturbations to orders ϵ^2 and α^2 .

The stability of out-of-plane perturbations is governed by the sign of $\mathcal{H}^{(2,0)}$, which depends not only on ϕ , but also the material properties of the solvating polymer (R_0 , k_g , k_n , and q_0), the membrane bending moduli (κ and $\bar{\kappa}$), and the membrane tension σ , which is set during formation. We focus on how the properties of the membrane

(*i.e.*, tension and bending) affect discoid stability and, in particular, the role of $\bar{\kappa}$. Leaving the details to the SM, we write $\mathcal{H}^{(2,0)} = \pi \phi [\bar{\kappa} - \bar{\kappa}^*(\phi)]$, which introduces a critical value of Gaussian rigidity, $\bar{\kappa}^*$. Fig. 3 shows how this quantity determines the stability of a given perturbation ϕ , as a function of the ratio $\bar{\kappa}/\kappa$. Also shown is the magnitude of $\mathcal{H}^{(2,0)}$, and hence the rate at which the perturbation grows or shrinks in time. For a band of values of $\bar{\kappa}/\kappa$, all perturbations are suppressed and only flat discs are stable. Outside of this band, perturbations characterised by a range of ϕ are unstable. However, the dominant (*i.e.*, fastest growing) mode always corresponds to either $\phi = -1$ or $\phi = +1$. That is, a saddle with principal curvatures of equal magnitude— a “pringle”— or a shallow section of a sphere, respectively. In the case of the former, the instability that takes a flat disc to a pringle is just $\bar{\kappa} \geq \bar{\kappa}_p^*$, where the critical value

$$\bar{\kappa}_p^* = \left(\frac{3}{2 R_0} - q_0 \right) k_g + \frac{k_n}{2 R_0} - \frac{R_0^2 \sigma}{4}, \quad (7)$$

is marked in Fig. 3. For a given $\bar{\kappa}$ therefore, pringles are always unstable for tensions above some critical value σ_p , which can be found by inverting (7).

We can assess whether such tensions $\sigma \geq \sigma_p(\bar{\kappa})$ are physically plausible by analysing cryo-Electron Microscopy images of SMA stabilised discoids. When combined with equipartition (4), such images permit the calculation of an effective upper bound on σ_p by estimating the maximum possible values of k_g and k_n . Figure 4 shows one such cryo-EM image, prepared according to [4]— *i.e.*, stabilised by SMA and cut from moderate tension vesicles ($\sigma \sim 10^{-4} \text{ N/m}$) that were synthesised from *E. Coli* lipid extract ($\bar{\kappa} \simeq -\kappa$ [22]). For such systems, if k_g is sufficiently large to stabilise the fluctuations in projected discoid shape and size ($\geq R_0^3 \sigma/3$), then out of plane fluctuations are also suppressed if $k_n \geq k_g$. (That is, the line $\bar{\kappa} = -\kappa$ is within the grey region of Fig. 3). In

this case, equilibrium discoids are flat discs, and any variation in shape appearing in Fig. 4 is a result of projection onto the focal plane. Using image processing, each discoid may be fitted to an ellipse, and the mean-squared deviation of the semi-major axes may be calculated (Fig. 4 and SM). The result can be used to invert Eq. (4) at $n = 0$ and predict an upper estimate for the geodesic rigidity of $k_g = 7 k_B T \text{ nm}$. Further assuming $k_g = k_n$ and setting $q_0 = 1/R_0$, the aforementioned upper estimate for k_g yields an *upper* bound on σ_p of $\sim 10^{-2} \text{ N/m}$, a tension at which bilayer membranes typically rupture [?]. We deduce, therefore, that pringle-shaped discoids can likely be cut from L_α phase membrane at large, but physically plausible, tensions. Moreover, by considering higher order contributions to the energy, it can be shown that the resultant pringles are stable for moduli of Gaussian rigidity $\bar{\kappa} \geq \max(\bar{\kappa}_p^*, \bar{\kappa}_p^\dagger)$ (see SM), where $\bar{\kappa}_p^\dagger$ a critical value similar to that of Eq. (7), but which is determined at $O(\alpha^4)$.

IV. FRACTIONATION ACCORDING TO MODULUS OF GAUSSIAN CURVATURE

Significantly, the pringle transition can occur *before* the bulk membrane phase switches from lamellar (L_α) to sponge (L_3) [15]. That is, saddle-shaped discoids can form spontaneously after being cut from flat sheets, as opposed to being cut from a bilayer with equilibrium negative Gaussian curvature, such as the sponge phase. Stable pringles are interesting because they promote the preferential sorting of lipids with larger intrinsic Gaussian rigidities into the discoids as they are formed. To illustrate this we consider a simple two-component model in which an SMA stabilised pringle emerges from a well-mixed (bulk) membrane having an average Gaussian rigidity $\bar{\kappa}$ in the regime $\bar{\kappa} > \max(\bar{\kappa}_p^*, \bar{\kappa}_p^\dagger)$. Relative to the bulk membrane, the pringle may contain an additional area fraction ψ of one of the components, resulting in a Gaussian rigidity for the pringle of the form $\bar{\kappa} + \delta\bar{\kappa}\psi$, with $\delta\bar{\kappa} = \bar{\kappa}_1 - \bar{\kappa}_2 > 0$ the difference between the Gaussian rigidity of each component. The membrane Hamiltonian might then include an extra term

$$\mathcal{H}_\psi = \int_S \frac{\chi \psi^2}{2} dA, \quad (8)$$

with χ a Flory parameter that approaches zero as the bulk membrane approaches the demixing transition. The inclusion of (8) implies that the disc spontaneously adopts the shape of a stable pringle, with curvature given by

$$|c_1| = \frac{1}{R_0} \left[\frac{2(\bar{\kappa} - \bar{\kappa}_p^*)}{3(\bar{\kappa} - \bar{\kappa}_\chi^\dagger)} \right]^{1/2}, \quad (9)$$

when $\bar{\kappa} > \max(\bar{\kappa}_p^*, \bar{\kappa}_\chi^\dagger)$ for $\bar{\kappa}_\chi^\dagger = \bar{\kappa}_p^\dagger - 2(\delta\bar{\kappa})^2/\chi R_0^2$ (see SM). The corresponding equilibrium composition of the

discoid is characterised by the additional area fraction

$$\psi = \frac{2\delta\bar{\kappa}(\bar{\kappa} - \bar{\kappa}_p^*)}{3\chi R_0^2(\bar{\kappa} - \bar{\kappa}_\chi^\dagger)}, \quad (10)$$

which is occupied by lipids with modulus of Gaussian rigidity $\bar{\kappa}_1$.

V. CONCLUSIONS AND DISCUSSION

Taken as a whole, our analysis suggests the possibility of using lipid nanodiscoids to not only phase-separate, but actually *fractionate* membrane components by $\bar{\kappa}$; those components with the largest values of $\bar{\kappa}$ will be preferentially sorted into pringles. It is also possible that the instability described here could be used as the basis of a technique to measure or compare values of $\bar{\kappa}$. One possible approach is to slowly increase the surface tension of vesicles via micropipette-aspiration or osmotic control: saddle shapes should first form when $\bar{\kappa} = \bar{\kappa}_p^*(\sigma)$. We reiterate that these results are especially pertinent given the lack of available alternatives that prob lipid coupling to membrane Gaussian curvature.

We propose that such ideas can readily be extended to areas of significant Biological interest: the localisation or activities of membrane-bound proteins may also depend on Gaussian curvature via both the protein's effective shape and elastic response to deformation. Indeed, given that membrane-bound proteins can be co-solvated with their integrity preserved, the nanoscale discoids described here provide an interesting new quantitative technology for studying the wider role of Gaussian curvature in cell Biology— *e.g.*, the sorting and function of membrane-bound proteins in organelles whose function is closely tied to morphology, such as the Endoplasmic Reticulum or Golgi Apparatus. We therefore welcome further work in the area.

Acknowledgments

R.G.M and M.S.T acknowledge the support of EPSRC grant # EP/E501311/1, a Leadership fellowship to M.S.T. R.G.M also acknowledges the Simons Foundation and the Tata Institute of Fundamental Research. T.R.D acknowledges the support of a BBSRC BRIC project grant # BB/G010412/1.

Author contributions

M.S.T and T.R.D conceived-of and designed the research. R.G.M and M.S.T performed analysis and T.R.D contributed images/data. R.G.M and M.S.T wrote the manuscript in consultation with T.R.D.

- [1] T. J. Knowles, R. Finka, C. Smith, Y.-P. Lin, T. R. Dafforn, and M. Overduin. Membrane Proteins Solubilized Intact in Lipid Containing Nanoparticles Bounded by Styrene Maleic Acid Copolymer. *J. Am. Chem. Soc.*, 131(22):7484–7485, 2009.
- [2] S. Tonge, V. Rebeix, and B. J. Tighe. Dynamic Surface Activity of Biological Fluids and Ophthalmic Solutions. *Cornea*, 19(Supplement 2):S133, 2000.
- [3] S. R. Tonge and B. J. Tighe. Responsive hydrophobically associating polymers: a review of structure and properties. *Adv. Drug Deliv. Rev.*, 53(1):109–122, 2001.
- [4] S. C. Lee, T. J. Knowles, V. L. G. Postis, M. Jamshad, R. A. Parslow, Y.-P. Lin, A. Goldman, P. Sridhar, M. Overduin, S. P. Muench, and T. R. Dafforn. A method for detergent-free isolation of membrane proteins in their local lipid environment. *Nat. Protoc.*, 11(7):1149–1162, 2016.
- [5] T. H. Bayburt, Y. V. Grinkova, and S. G. Sligar. Self-Assembly of Discoidal Phospholipid Bilayer Nanoparticles with Membrane Scaffold Proteins. *Nano Lett.*, 2(8):853–856, 2002.
- [6] M. A. Schuler, I. G. Denisov, and S. G. Sligar. Nanodiscs as a New Tool to Examine LipidProtein Interactions. In Jörg H. Kleinschmidt, editor, *Lipid Protein Interact.*, pages 415–433. Springer, New York, 2013.
- [7] I. G. Denisov and S. G. Sligar. Nanodiscs for structural and functional studies of membrane proteins. *Nat. Struct. Mol. Biol.*, 23(6):481–486, 2016.
- [8] M. Orwick-Rydmark, J. E. Lovett, A. Graziadei, L. Lindholm, M. R. Hicks, and A. Watts. Detergent-Free Incorporation of a Seven-Transmembrane Receptor Protein into Nanosized Bilayer Lipodisc Particles for Functional and Biophysical Studies. *Nano Lett.*, 12(9):4687–4692, 2012.
- [9] S. Paulin, M. Jamshad, T. R. Dafforn, J. Garcia-Lara, S. J. Foster, N. F. Galley, D. I. Roper, H. Rosado, and P. W. Taylor. Surfactant-free purification of membrane protein complexes from bacteria: application to the staphylococcal penicillin-binding protein complex PBP2/PBP2a. *Nanotechnology*, 25(28):285101, 2014.
- [10] J. M. Dörr, M. C. Koorengevel, M. Schäfer, A. V. Prokofyev, S. Scheidelaar, E. A. W. van der Cruysen, T. R. Dafforn, M. Baldus, and J. A. Killian. Detergent-free isolation, characterization, and functional reconstitution of a tetrameric K⁺ channel: The power of native nanodiscs. *Proc. Natl. Acad. Sci.*, 111(52):18607–18612, 2014.
- [11] S. Gulati, M. Jamshad, T. J. Knowles, K. A. Morrison, R. Downing, N. Cant, R. Collins, J. B. Koenderink, R. C. Ford, M. Overduin, I. D. Kerr, T. R. Dafforn, and A. J. Rothnie. Detergent-free purification of ABC (ATP-binding-cassette) transporters. *Biochem. J.*, 461(2):269–278, 2014.
- [12] V. Postis, S. Rawson, J. K. Mitchell, S. C. Lee, R. A. Parslow, T. R. Dafforn, S. A. Baldwin, and S. P. Muench. The use of SMALPs as a novel membrane protein scaffold for structure study by negative stain electron microscopy. *Biochim. Biophys. Acta - Biomembr.*, 1848(2):496–501, 2015.
- [13] C. Sun, S. Benlekbir, P. Venkatakrishnan, Y. Wang, S. Hong, J. Hosler, E. Tajkhorshid, J. L. Rubinstein, and R. B. Gennis. Structure of the alternative complex III in a supercomplex with cytochrome oxidase. *Nature*, 557(7703):123–126, 2018.
- [14] W. Qiu, Z. Fu, G. G. Xu, R. A. Grassucci, Y. Zhang, J. Frank, W. A. Hendrickson, and Y. Guo. Structure and activity of lipid bilayer within a membrane-protein transporter. *Proc. Natl. Acad. Sci.*, 115(51):12985–12990, 2018.
- [15] S. A. Safran. *Statistical Thermodynamics of Surfaces, Interfaces and Membranes*. Perseus, Cambridge, MA, 1994.
- [16] W. Helfrich. Elastic properties of lipid bilayers: theory and possible experiments. *Z. Naturforsch.*, 28(c):693–703, 1973.
- [17] M. P. do Carmo. *Differential Geometry of Curves and Surfaces*. Prentice-Hall, New Jersey, 1976.
- [18] M. S. Turner and P. Sens. Gating-by-Tilt of Mechanically Sensitive Membrane Channels. *Phys. Rev. Lett.*, 93(11):118103, 2004.
- [19] B. Alberts, D. Bray, J. Lewis, M. Raff, K. Roberts, and J. D. Watson. *Molecular biology of the cell*. Garland Science, New York, 1989.
- [20] J. Nixon-Abell, C. J. Obara, A. V. Weigel, D. Li, W. R. Legant, C. S. Xu, H. A. Pasolli, K. Harvey, H. F. Hess, E. Betzig, C. Blackstone, and J. Lippincott-Schwartz. Increased spatiotemporal resolution reveals highly dynamic dense tubular matrices in the peripheral ER. *Science (80-.)*, 354(6311):aaf3928, 2016.
- [21] P. G. De Gennes and Pros. *The Physics of Liquid Crystals*. Oxford University Press, Oxford, 1993.
- [22] M. Hu, J. J. Briguglio, and M. Deserno. Determining the Gaussian Curvature Modulus of Lipid Membranes in Simulations. *Biophys. J.*, 102(6):1403–1410, mar 2012.
- [23] P. M. Chaikin and T. C. Lubensky. *Principles of Condensed Matter Physics*. Cambridge University Press, Cambridge, England, 1995.
- [24] T. Frankel, *The Geometry of Physics: An Introduction* 3rd Ed. (Cambridge University Press, Cambridge, UK, 2012).
- [25] Wolfram Research, Inc., Mathematica, Version 10.1, Champaign, IL (2015).

SUPPLEMENTARY MATERIAL

INTRODUCTION

The purpose of this supplementary material is threefold. First, to provide any necessary theoretical background (in a terse, but self-contained way), particularly with respect to differential geometry (for further details, the reader is referred to [17, 24]). Second, to provide a detailed account (making heavy use of the aforementioned background) of the calculations whose results appear in the main manuscript. Lastly, to describe the protocol used to analyse the cryo Electron Microscopy images.

GEOMETRY

Setup and notation

Let \mathcal{S} be a smooth Riemannian manifold representing the nanodiscoid midsurface. If points on the midsurface are labelled by an “internal” coordinate $u \in \mathbb{R}^2$, then \mathcal{S} is just the image of u under an embedding $F : \mathbb{R}^2 \rightarrow \mathbb{R}^3$. That is, the position in \mathbb{R}^3 of a point u is given by the vector $\mathbf{R}(u) =: F(u)$.

In terms of notation, the convention, which will be used throughout, is that Greek indices take values 1 or 2, whilst Latin indices take 1, 2 or 3. Bold typeface is used to represent vectors in \mathbb{R}^3 , such that $\mathbf{v} = v^i \hat{\mathbf{e}}_i$, where an implicit sum is understood by repeated indices of different type (*i.e.*, upper and lower), and $\{\hat{\mathbf{e}}_i : i = 1, 2, 3\}$ are the usual normalised basis vectors, independent of position $\mathbf{R}(u)$. By contrast, an overarrow is used for vectors in \mathbb{R}^2 , such that $\vec{v} = v^\alpha \vec{e}_\alpha$, with $\{\vec{e}_\alpha : \alpha = 1, 2\}$ representing non-normalised basis vectors, which depend on position u .

The embedding F corresponds to a pushforward $F_* : T_u \mathbb{R}^2 \rightarrow T_{\mathbf{R}(u)} \mathbb{R}^3$, whose operation is defined by:

$$\mathbf{F}_*(\vec{e}_\alpha) = \frac{\partial \mathbf{R}(u^\alpha)}{\partial u^\alpha}. \quad (11)$$

The notion of $\mathbf{F}_*(\vec{e}_\alpha)$ can be used to define the unit normal to \mathcal{S} :

$$\hat{\mathbf{n}} = \frac{\mathbf{F}_*(\vec{e}_1) \times \mathbf{F}_*(\vec{e}_2)}{|\mathbf{F}_*(\vec{e}_1) \times \mathbf{F}_*(\vec{e}_2)|}, \quad (12)$$

where the symbol \times represents the usual cross product in \mathbb{R}^3 . (For the purposes of this article, it suffices to assume that the orientation of the basis of a manifold is the same as the orientation of the manifold itself).

Forms

A form $r^{(k)}$ of degree k is a linear functional that takes k tangent vectors and returns a real number. For example, a 0-form is a function, a 1-form is a co-vector, and higher forms of degree k are tensors of rank $(0, k)$. (For notation, the degree of a form will be indicated by a bracketed superscript unless explicitly stated otherwise).

1-forms

At a point u , the basis of 1-forms that spans the cotangent space, $T_u^* \mathbb{R}^2$, is given by $\{du^\alpha : \alpha = 1, 2\}$, such that $du^\alpha(\vec{e}_\beta) = \delta_\beta^\alpha$, where δ_β^α is the Kronecker delta symbol. In this basis, $p = p_\alpha du^\alpha$, where once again there is an implicit sum over repeated indices.

For example, consider a curve \mathcal{C} , parameterised by t and embedded in \mathcal{S} . \mathcal{C} has tangent vectors $\mathbf{T} = \partial \mathbf{R} / \partial t$ with pre-image \vec{T} under F_* . In this case, the line element “ dl ” is just

$$dl := \left\| \vec{T} \right\| dt = [g_{\alpha\beta} T^\alpha T^\beta]^{1/2} dt. \quad (13)$$

Equivalently, “ dl ” can also be defined relative to the Euclidean coordinates of the embedding space:

$$dl = \left\{ \delta_{ij} [\mathbf{F}_*(\vec{T})]^i [\mathbf{F}_*(\vec{T})]^j \right\}^{1/2} dt, \quad (14)$$

where the implied sum is now over $i, j = 1, 2, 3$ and not $\alpha, \beta = 1, 2$ as in (13) and δ_{ij} is just the metric in Euclidean coordinates.

First fundamental form, metric and inner product

The embedding function F induces a metric on \mathbb{R}^2 via the pullback F^* . That is $g_{\alpha\beta}(u) = (F^* \mathbf{I})(\vec{e}_\alpha, \vec{e}_\beta) = \mathbf{F}_*(\vec{e}_\alpha) \cdot \mathbf{F}_*(\vec{e}_\beta)$, where \mathbf{I} is the first fundamental form of \mathbb{R}^3 (*i.e.*, with coefficients δ^{ij}) and “ \cdot ” is the usual dot product. At each point $u \in \mathbb{R}^2$, the induced metric can be used to define an inner product $\langle \cdot, \cdot \rangle : T_u \mathbb{R}^2 \times T_u \mathbb{R}^2 \rightarrow \mathbb{R}$. That is, for arbitrary vectors \vec{v} and \vec{w} , we define $\langle \vec{v}, \vec{w} \rangle := v^\alpha g_{\alpha\beta} w^\beta$. Such an inner product permits the explicit identification of a vector, *e.g.*, \vec{v} , with its dual 1-form, v , by the condition $v(\vec{w}) = \langle \vec{v}, \vec{w} \rangle$, which holds for all \vec{w} . Noticing that $v(\vec{w}) = v_\alpha du^\alpha(\vec{w}) = v_\alpha w^\alpha$ and using the above definition of the inner product of two vectors implies the raising and lowering properties of the metric and its inverse [$g^{\alpha\beta} = (g_{\alpha\beta})^{-1}$], respectively. That is, $v_\alpha = g_{\alpha\beta} v^\beta$ and $v^\alpha = g^{\alpha\beta} v_\beta$. Using this property, the inner product acting on two 1-forms can be defined in a complementary way to that of the inner product on vectors:

$$\langle v, w \rangle := v_\alpha g^{\alpha\beta} w_\beta = v_\alpha w^\alpha = \langle \vec{v}, \vec{w} \rangle. \quad (15)$$

Covariant derivative

The covariant derivative at a point u on S is a generalisation of the directional derivative. It calculates the rate of change of a tensor field (at u) whilst moving along the unique geodesic that has tangent vector with pre-image \vec{y} (at u) under F_* .

Scalars

The action of the covariant derivative on a scalar field ϕ is defined to be

$$\nabla_{\vec{y}} \phi := \phi_{,\alpha} du^\alpha(\vec{y}), \quad (16)$$

where a subscript comma “ $,$ ” is shorthand for a partial derivative, *i.e.*, $\phi_{,\alpha} := \partial\phi/\partial u^\alpha$.

Vectors

When acting on a tangent vector $\vec{v} = v^\alpha \vec{e}_\alpha$, we write

$$\nabla_{\vec{y}} \vec{v} := \vec{e}_\alpha (v^\alpha{}_{;\beta}) du^\beta(\vec{y}), \quad (17)$$

where the components $v^\alpha{}_{;\beta}$ are given by

$$v^\alpha{}_{;\beta} := v^\alpha{}_{,\beta} + v^\gamma \Gamma_{\beta\gamma}^\alpha. \quad (18)$$

Once again, a subscript comma “ $,$ ” is shorthand for a partial derivative, $v^i{}_{,j} := \partial v^i / \partial u^j$, whilst the $\Gamma_{\beta\gamma}^\alpha = g^{\alpha\delta} (g_{\delta\beta,\gamma} + g_{\delta\gamma,\beta} - g_{\beta\gamma,\delta}) / 2$ are Christoffel symbols, which define the action of the covariant derivative, via $\nabla_{\vec{e}_\alpha} \vec{e}_\beta = \vec{e}_\gamma \Gamma_{\alpha\beta}^\gamma$. Note that the shorthand $\nabla_\alpha := \nabla_{\vec{e}_\alpha}$ is frequently used in physics.

1-forms

For a 1-form, the action of the covariant derivative can be defined by demanding that the “Leibniz rule” holds. That is, if a scalar field is defined by the action of a 1-form on a vector, *i.e.*, $\phi := v(\vec{w}) = v^\alpha w_\alpha$, then

$$\nabla_\alpha (v^\beta w_\beta) = (v^\beta w_\beta)_\alpha := v^\beta{}_{;\alpha} w_\beta + v^\beta w_{\beta;\alpha}. \quad (19)$$

The result is that $v_{\alpha;\beta} := v_{\alpha,\beta} - v_\gamma \Gamma_{\alpha\beta}^\gamma$, which is consistent with the notion of using the metric as a raising / lowering operator (*i.e.*, $v_{\alpha;\beta} = g_{\alpha\gamma} v^\gamma{}_{;\beta}$). In coordinate free notation, this is equivalent to

$$(\nabla_{\vec{y}} v)(\vec{w}) := \nabla_{\vec{y}} [v(\vec{w})] - v(\nabla_{\vec{y}} \vec{w}). \quad (20)$$

Second fundamental form, Gauss and Weingarten equations

Consider the derivative

$$\frac{\partial \hat{\mathbf{n}}}{\partial u^\alpha} =: \hat{\mathbf{n}}_{,\alpha}, \quad (21)$$

i.e., the rate (and direction) of change in the unit normal to \mathcal{S} as u^α is varied, expressed as a vector in \mathbb{R}^3 . Since $\hat{\mathbf{n}}$ is a unit vector, the result must still be tangent to \mathcal{S} and therefore

$$\hat{\mathbf{n}}_{,\alpha} = -b^\beta_\alpha \mathbf{F}_*(\vec{e}_\beta), \quad (22)$$

which is known as the Weingarten equation (the assignment of a minus sign being convention). Given the right-hand side, we can use the coefficients from the above to construct a linear map $b : T\mathbb{R}^2 \rightarrow T\mathbb{R}^2$ by writing $\vec{b}(\vec{v}) = -v^\beta \vec{e}_\beta b^\alpha_\beta$, for arbitrary \vec{v} . Similarly, there is a natural bilinear form Π , known as the *second fundamental form*, that can be associated with such a map, whose action is given by

$$\Pi(\vec{v}, \vec{w}) = \langle \vec{v}, \vec{b}(\vec{w}) \rangle = v^\gamma w^\beta \langle \vec{e}_\gamma, -b^\alpha_\beta \vec{e}_\alpha \rangle. \quad (23)$$

That is

$$\Pi = -[\mathbf{F}_*(\vec{e}_\alpha) \cdot \hat{\mathbf{n}}_{,\beta}] du^\alpha \otimes du^\beta = b_{\alpha\beta} du^\alpha \otimes du^\beta, \quad (24)$$

where $b_{\alpha\beta} = g_{\alpha\gamma} b^\gamma_\beta = -[\mathbf{F}_*(\vec{e}_\alpha) \cdot \hat{\mathbf{n}}_{,\beta}]$. Notice that since $\partial[\mathbf{F}_*(\vec{e}_\alpha) \cdot \hat{\mathbf{n}}]/\partial u^\beta = 0$, we have $b_{\alpha\beta} = (\partial \mathbf{F}_*(\vec{e}_\alpha)/\partial u^\beta) \cdot \hat{\mathbf{n}}$. More generally, the derivative of basis vectors \vec{e}_α with respect to some coordinate u^β on \mathcal{S} can be decomposed into tangent and normal parts.

$$\frac{\partial \mathbf{F}_*(\vec{e}_\alpha)}{\partial u^\beta} = \Gamma^\gamma_{\alpha\beta} \mathbf{F}_*(\vec{e}_\gamma) + b_{\alpha\beta} \hat{\mathbf{n}}, \quad (25)$$

which is known as Gauss' equation.

Curvature

Lines

In \mathbb{R}^3 , the curvature q of a line $\gamma(t)$ at a given point x is just the norm of the covariant derivative acting on the unit tangent to the line (in the direction tangent to γ) at x :

$$q := \|\nabla_{\hat{\mathbf{T}}} \hat{\mathbf{T}}\| = \left[\delta_{ij} \left(\nabla_{\hat{\mathbf{T}}} \hat{\mathbf{T}} \right)^i \left(\nabla_{\hat{\mathbf{T}}} \hat{\mathbf{T}} \right)^j \right]^{1/2}, \quad (26)$$

where

$$\hat{\mathbf{T}} = \left\| \frac{d\gamma}{dt} \right\|^{-1} \frac{d\gamma}{dt}, \quad (27)$$

are just normalised tangent vectors to $\gamma(t)$ and the covariant derivative reduces to the usual directional derivative of \mathbb{R}^3 , *i.e.*, $\hat{\mathbf{T}} \cdot (\partial/\partial x, \partial/\partial y, \partial/\partial z)^\top$.

For lines that are also embedded in a sub-manifold (*e.g.*, the boundary $\partial\mathcal{S}$ is a line in both \mathbb{R}^3 and \mathcal{S}) there are two common measures of curvature: geodesic and normal. The geodesic curvature is a measure of curvature in the tangent plane $T\mathcal{S}$. That is

$$q_g := \|\nabla_{\hat{\hat{T}}} \hat{\hat{T}}\| = \left[g_{\alpha\beta} \left(\nabla_{\hat{\hat{T}}} \hat{\hat{T}} \right)^\alpha \left(\nabla_{\hat{\hat{T}}} \hat{\hat{T}} \right)^\beta \right]^{1/2}, \quad (28)$$

where $\hat{\hat{T}}$ is the pre-image of $\hat{\mathbf{T}}$ under F_* . By contrast to (28), the normal curvature measures the out-of-(sub)manifold curvature and is given by

$$q_n := \left[\delta_{ij} \left\{ \left[\left(\nabla_{\hat{\mathbf{T}}} \hat{\mathbf{T}} \right) \cdot \hat{\mathbf{n}} \right] \hat{\mathbf{n}} \right\}^i \left\{ \left[\left(\nabla_{\hat{\mathbf{T}}} \hat{\mathbf{T}} \right) \cdot \hat{\mathbf{n}} \right] \hat{\mathbf{n}} \right\}^j \right]^{1/2}. \quad (29)$$

Both q_g and q_n are linked to q via the following relation

$$q = \sqrt{q_g^2 + q_n^2}. \quad (30)$$

Surfaces

At a given point $p \in \mathbb{R}^2$, each unit vector $\hat{\mathbf{y}}$ corresponds to a unique curve C on \mathcal{S} that also lies in the plane \mathcal{P} spanned by $\hat{\mathbf{n}}$ and $\mathbf{F}_* \left(\hat{\mathbf{y}} \right)$. The action of the second fundamental form on a given $\hat{\mathbf{y}}$, results in the *normal* curvature $c_{\hat{\mathbf{y}}}^{(n)}$ of \mathcal{S} in the direction of $\mathbf{F}_* \left(\hat{\mathbf{y}} \right)$ (*i.e.*, the curvature of C in \mathcal{P}). We write,

$$\Pi(\hat{\mathbf{y}}, \hat{\mathbf{y}}) = \pm c_{\hat{\mathbf{y}}}^{(n)}, \quad (31)$$

where “+” indicates whether C is curving towards the unit normal, and *vice-versa* for “-”. Since the normal curvature will change dependent on which direction $\hat{\mathbf{y}}$ is chosen, we define the principal directions:

$$\hat{\mathbf{y}}_1(p) = \arg \max_{\hat{\mathbf{y}} \in T_p \mathbb{R}^2} \Pi(\hat{\mathbf{y}}, \hat{\mathbf{y}}), \text{ and } \hat{\mathbf{y}}_2(p) = \arg \min_{\hat{\mathbf{y}} \in T_p \mathbb{R}^2} \Pi(\hat{\mathbf{y}}, \hat{\mathbf{y}}). \quad (32)$$

The principal curvatures are then given by

$$c_\alpha(p) = \Pi(\hat{\mathbf{y}}_\alpha, \hat{\mathbf{y}}_\alpha), \quad \forall \alpha = 1, 2. \quad (33)$$

It can be shown that the c_α are eigenvalues of the linear operator \vec{b} from §V. That is,

$$\vec{b}(\hat{\mathbf{y}}_\alpha) = c_\alpha \hat{\mathbf{y}}_\alpha, \quad (34)$$

where if $c_1 \neq c_2$, the principal directions are orthogonal. We may now define two different types of local curvature of \mathcal{S} : the *mean* curvature

$$H := \frac{1}{2} \text{Tr } b^\alpha_\beta = \frac{1}{2} \text{Tr}_g \Pi = \frac{c_1 + c_2}{2}, \quad (35)$$

and the *Gaussian* curvature

$$K := \text{Det } b^\alpha_\beta = \frac{\text{Det } b_{\alpha\beta}}{\text{Det } g_{\alpha\beta}} = c_1 c_2. \quad (36)$$

SOLVATED MEMBRANE NANODISCOIDS

Consider a nanoscale bilayer discoid, stabilised by a solvating compound such as Styrene Maleic Acid or the lipoprotein APO-1A. Write $\mathcal{H} = \mathcal{H}_m + \mathcal{H}_b$, where

$$\mathcal{H}_m = \int_{\mathcal{S}} dA \left[\sigma + \frac{\kappa}{2} (2H - c_0)^2 + \bar{\kappa} K \right], \quad (37)$$

and

$$\mathcal{H}_b = \int_{\partial \mathcal{S}} dl \left[\tau + \frac{k_g}{2} (q_g - q_0)^2 + \frac{k_n}{2} q_n^2 \right], \quad (38)$$

are energetic contributions from the bilayer membrane and solvating compound, respectively. In the first integral (37), dA is the surface area element of \mathcal{S} , H and K are the mean [*cf.* Eq. (35)] and Gaussian [*cf.* Eq. (36)] curvatures respectively, and σ is a surface tension. The moduli κ and $\bar{\kappa}$ are the bending and Gaussian (saddle-splay) rigidities, respectively, and c_0 is the membrane’s spontaneous (mean) curvature. In the second integral (38), dl is the line element [*cf.* Eq. (13)] of the surface boundary $\partial \mathcal{S}$, τ is a line tension, q_g is the geodesic curvature [*cf.* Eq. (28)], and q_n is the normal curvature [*cf.* Eq. (29)]. The coefficients k_g and k_n are corresponding bending moduli with dimensions of energy multiplied by length. The SMA co-polymer is assumed to have spontaneous (line) curvature q_0 in the tangent plane to the disc, but not in the normal direction (*i.e.*, it preserves the up-down symmetry of the bilayer). Restricting the analysis to surfaces with an Euler characteristic of one, the Gauss-Bonnet theorem gives:

$$\int_{\mathcal{S}} K dA = \int_{\partial \mathcal{S}} k_g dl + 2\pi. \quad (39)$$

Substituting into (37) and (38), we have

$$\mathcal{H} = \int_{\mathcal{S}} dA \left[\sigma + \frac{\kappa}{2} (2H - c_0)^2 + \bar{\kappa}_g K \right] + \int_{\partial \mathcal{S}} dl \left[\tau_g + \frac{k_g}{2} q_g^2 + \frac{k_n}{2} q_n^2 \right] - k_g q_0 2\pi. \quad (40)$$

where $\bar{\kappa}_k := \bar{\kappa} + q_0 k$ and $\tau_k := \tau + k q_0^2/2$ are re-normalised constants.

Flat

Assume that $H = K = c_0 = q_n = 0$, which implies \mathcal{S} is just some bounded domain in \mathbb{R}^2 and only the line integral of (40) needs to be calculated. Using polar coordinates (r, θ) it is assumed that the discoid boundary $\partial\mathcal{S}$ can be characterised by the vector field $\vec{\gamma}(\theta)$, which is taken to be single-valued. Throughout, we use the convention that the magnitude of a vector is indicated by omitting the overarrow, *i.e.*, $\gamma(\theta) = \|\vec{\gamma}(\theta)\|$. In the natural basis $\vec{e}_1 = \hat{r}$ and $\vec{e}_2 = r\hat{\theta}$, the set of vectors tangent to the line $\vec{\gamma}(\theta)$, are just given by $d\vec{\gamma}/d\theta = \gamma\vec{e}_1 + \vec{e}_2$. The metric is just that of \mathbb{R}^2 in polar coordinates, *i.e.*, $g_{\alpha\beta} = \text{Diag}[1, r^2]$. The “line element” dl [cf. Eq. (13)] is then given by

$$dl = \left[\gamma^2 + \left(\frac{d\gamma}{d\theta} \right)^2 \right]^{1/2} d\theta. \quad (41)$$

Similarly, the normalised vectors tangent to $\partial\mathcal{S}$ are given by

$$\hat{T} = \frac{1}{\sqrt{\gamma^2 + (d\gamma/d\theta)^2}} \left(\frac{d\gamma}{d\theta}, 1 \right)^T. \quad (42)$$

Here, since the Christoffel symbols Γ_{jk}^i are only non-zero in three cases: $\Gamma_{22}^1 = -r$, and $\Gamma_{12}^2 = \Gamma_{21}^2 = 1/r$, the components of the covariant derivative $\nabla_{\hat{T}} \hat{T}$ are

$$\left(\nabla_{\hat{T}} \hat{T} \right)^1 = -\frac{\gamma \left[\gamma^2 + 2(\gamma')^2 - \gamma\gamma'' \right]}{\left[\gamma^2 + (\gamma')^2 \right]^2}, \quad \text{and} \quad \left(\nabla_{\hat{T}} \hat{T} \right)^2 = \frac{\gamma' \left[\gamma^2 + 2(\gamma')^2 - \gamma\gamma'' \right]}{\gamma \left[\gamma^2 + (\gamma')^2 \right]^2}, \quad (43)$$

where the shorthand $\gamma' = d\gamma/d\theta$ has been introduced for readability. Returning to (28), we see that

$$q_g = \frac{\gamma^2 + 2(\gamma')^2 - \gamma\gamma''}{\left[\gamma^2 + (\gamma')^2 \right]^{3/2}}. \quad (44)$$

If the membrane boundary is quasi-circular, then $\gamma(\theta) = R_0 [1 + \epsilon f(\theta)]$, where $f(\theta) = \sum_n \Re [A_n \exp(in\theta)]$, such that \Re is the real part, $A_n \in \mathbb{C}$, $|A_n| \leq 1 \forall n \in \mathbb{N}$, and $\epsilon \ll 1$. A power series expansion in ϵ can then be performed on Eqs. (41) and (44), with the results

$$dl = R_0 \left\{ 1 + \epsilon \sum_n \Re [A_n \exp(in\theta)] + \frac{\epsilon^2}{2} \sum_n n \Re [i A_n \exp(in\theta)]^2 \right\} d\theta + O(\epsilon^3), \quad (45)$$

and

$$q_g = \frac{1}{R_0} \left\{ 1 + \epsilon \sum_n (n^2 - 1) \Re [\exp(in\theta)] - \frac{\epsilon}{4} \sum_n \left\{ |A_n|^2 (3n^2 - 2) + \Re [A_n^2 \exp(2in\theta)] \right\} \right\} + O(\epsilon^3). \quad (46)$$

The energy \mathcal{H} can then be shown to be of the form

$$\begin{aligned} \mathcal{H} = \pi & \left[\frac{k_g (q_0 R_0 - 1)^2}{R_0} + R_0 (R_0 \sigma + 2\tau) \right] \\ & + \epsilon^2 \frac{\pi}{4R_0} \left\{ k_g [2 + (q_0^2 R_0^2 - 5) n^2 + 2n^4] + 2R_0^2 (R_0 \sigma + n^2 \tau) \right\} \sum_n |A_n|^2 + O(\epsilon^3). \end{aligned} \quad (47)$$

The minimum of \mathcal{H} is given by requiring $\partial\mathcal{H}/\partial R_0|_{\epsilon=0} = 0$. The result is that

$$\tau = \frac{k_g}{2R_0^2} (1 - q_0^2 R_0^2) - R_0 \sigma, \quad (48)$$

which implies

$$\mathcal{H} = \pi \left[\frac{k_g}{R_0} (1 - q_0 R_0) - \frac{R_0^2 \sigma}{2} \right] + \frac{\pi \epsilon^2}{2 R_0} \sum_n (n^2 - 1) [k_g (n^2 - 1) - R_0^3 \sigma] |A_n|^2 + O(\epsilon^3). \quad (49)$$

Notice that terms of $O(\epsilon^2)$ in Eq. (49) do *not* rely on q_0 , and therefore neither does the mean-squared amplitude of each mode in equilibrium.

The principle of equipartition of energy states that each quadratic mode contributes $k_B T/2$ to the expectation value of the energy— *i.e.*, summing \mathcal{H} over all configurations $\{A_n : n \in \mathbb{N}\}$, weighted by the Boltzmann distribution. Using angle brackets to indicate expectation value, this implies $\langle \mathcal{H}_n \rangle = k_B T/2$, where

$$\mathcal{H}_n = \frac{\pi \epsilon^2}{2 R_0} (n^2 - 1) [k_g (n^2 - 1) - R_0^3 \sigma] |A_n|^2. \quad (50)$$

Equation (3) in the main text then follows from the above.

Non-flat

Parameterise the membrane shape by using the two (orthogonal) principal curvatures, chosen without loss of generality such that $|c_1| \geq |c_2|$. The height field in an polar Monge approach is given by

$$h(r, \theta) = \frac{r^2}{4} [c_1 + c_2 + (c_1 - c_2) \cos 2\theta], \quad (51)$$

where the angle θ is assumed to be measured from the principal axis associated with c_1 . Moreover, $\|\nabla h\| \ll 1 \forall (r, \theta)$, therefore

$$\max \{\|\nabla h\| : \theta \in [0, 2\pi), r \in [0, \gamma(\theta)]\} = \|\nabla h\|_{\theta=0, r=\gamma(0)} = \gamma(0) c_1 \ll 1 \quad (52)$$

Since $\gamma(\theta) = R_0 [1 + \epsilon f(\theta)]$, we formally set $\alpha = R_0 c_1 \ll 1$, therefore (51) becomes

$$h(r, \theta) = \alpha \psi(r, \theta), \text{ with } \psi(r, \theta) = \frac{r^2}{4 R_0} [1 + \phi + (1 - \phi) \cos 2\theta], \quad (53)$$

where $\phi = c_2/c_1$ takes values in the interval $[-1, 1]$. Making contact with §V, \mathcal{S} is parameterised by $\{u^\alpha : \alpha = 1, 2\}$ and \mathbb{R}^3 by $\{x^i : i = 1, 2, 3\}$, where a Monge gauge is tantamount to choosing the map $\mathbf{F}(u) = (u^1, u^2, h(u^1, u^2))^T$. Moreover, $u^1 = r$ and $u^2 = \theta$, which implies that the embedding basis $\{\mathbf{e}_i : i = 1, 2, 3\}$ is just that of cylindrical polars $\{\hat{\mathbf{r}}, r\hat{\boldsymbol{\theta}}, \hat{\mathbf{z}}\}$. The position vector is then $\mathbf{R}(r, \theta) := r\hat{\mathbf{r}} + \alpha \psi(r, \theta)\hat{\mathbf{z}}$, and tangent vectors to the surface are spanned by the set:

$$\mathbf{F}_*(\vec{e}_1) = \frac{\partial \mathbf{R}}{\partial r} = \hat{\mathbf{r}} + \alpha \frac{\partial \psi}{\partial r} \hat{\mathbf{z}}, \text{ and } \mathbf{F}_*(\vec{e}_2) = \frac{\partial \mathbf{R}}{\partial \theta} = r\hat{\boldsymbol{\theta}} + \alpha \frac{\partial \psi}{\partial \theta} \hat{\mathbf{z}}. \quad (54)$$

Recalling the shorthand $\psi_{,\alpha} := \partial \psi / \partial u^\alpha$, the metric and its inverse become

$$g_{\alpha\beta} = \langle \vec{e}_\alpha, \vec{e}_\beta \rangle = \mathbf{F}_*(\vec{e}_\alpha) \cdot \mathbf{F}_*(\vec{e}_\beta) = \begin{pmatrix} 1 + \alpha^2 (\psi_{,1})^2 & \alpha^2 \psi_{,1} \psi_{,2} \\ \alpha^2 \psi_{,1} \psi_{,2} & r^2 + \alpha^2 (\psi_{,2})^2 \end{pmatrix}, \quad (55)$$

and

$$g^{\alpha\beta} = (g_{\alpha\beta})^{-1} = \frac{1}{r^2 (1 + \alpha^2 \|\nabla^{\mathbb{R}^2} \psi\|^2)} \begin{pmatrix} r^2 + \alpha^2 (\psi_{,2})^2 & -\alpha^2 \psi_{,1} \psi_{,2} \\ -\alpha^2 \psi_{,1} \psi_{,2} & 1 + \alpha^2 (\psi_{,1})^2 \end{pmatrix}. \quad (56)$$

It is clear that $g := \text{Det}(g_{\alpha\beta}) = r^2 \left(1 + \|\nabla^{\mathbb{R}^2} \psi\|^2\right)$, where $\nabla^{\mathbb{R}^2}$ is the covariant derivative in \mathbb{R}^2 (polar coordinates are assumed). We may also calculate the normal to the surface [*cf.* Eq. (12)],

$$\mathbf{n} = \hat{\mathbf{z}} \left(1 - \alpha^2 \|\nabla^{\mathbb{R}^2} \psi\|^2\right) - \hat{\mathbf{r}} \alpha \psi_{,1} - \hat{\boldsymbol{\theta}} \alpha \psi_{,2} + O(\alpha^3), \quad (57)$$

and the derivatives of the tangent vectors (pushed forwards to \mathbb{R}^3), *i.e.*,

$$\frac{\partial \mathbf{F}_* (\vec{e}_1)}{\partial u^1} = \frac{\partial^2 \mathbf{R}}{\partial r^2} = \alpha \psi_{,11} \hat{\mathbf{z}}, \quad \frac{\partial \mathbf{F}_* (\vec{e}_2)}{\partial u^2} = \frac{\partial^2 \mathbf{R}}{\partial \theta^2} = -r \hat{\mathbf{r}} + \alpha \psi_{,22} \hat{\mathbf{z}}, \quad \text{and} \quad \frac{\partial \mathbf{F}_* (\vec{e}_1)}{\partial u^2} = \frac{\partial^2 \mathbf{R}}{\partial r \partial \theta} = \hat{\boldsymbol{\theta}} + \alpha \psi_{,12} \hat{\mathbf{z}}, \quad (58)$$

from which the coefficients of the second fundamental form (24) may be constructed:

$$b_{\alpha\beta} = \alpha \begin{pmatrix} \psi_{,11} & \psi_{,12} - \psi_{,2}/r \\ \psi_{,12} - \psi_{,2}/r & r \psi_{,1} + \psi_{,22} \end{pmatrix} + O(\alpha^3). \quad (59)$$

Using the definitions (35) and (36) it can be shown that, up to second order in the small parameter α , the mean and Gaussian curvatures are just the trace and determinant of the (polar coordinate) Hessian of ψ . That is

$$H = \text{Tr} \left[\alpha \text{Hess}^{\mathbb{R}^2} (\psi) \right] + O(\alpha^3) = \frac{\alpha}{2} \left(\psi_{,11} + \frac{\psi_{,1}}{r} + \frac{\psi_{,22}}{r^2} \right) + O(\alpha^3) = \frac{\alpha}{2} \mathbb{R}^2 \nabla^2 \psi + O(\alpha^3), \quad (60)$$

and

$$K = \frac{1}{r^2} \text{Det} \left[\alpha \text{Hess}^{\mathbb{R}^2} (\psi) \right] + O(\alpha^3) = \frac{\alpha^2}{r^2} \left[\psi_{,11} (r \psi_{,1} + \psi_{,22}) - \left(\psi_{,12} - \frac{\psi_{,2}}{r} \right)^2 \right] + O(\alpha^3), \quad (61)$$

where

$$\left[\text{Hess}^{\mathbb{R}^2} (\psi) \right]_{\alpha\beta} := \psi_{,\alpha;\beta} = \psi_{,\alpha\beta} - \mathbb{R}^2 \Gamma_{\alpha\beta}^\gamma \psi_{,\gamma}. \quad (62)$$

Substituting for (53) leads to the results:

$$H = \frac{\alpha}{R_0} (1 + \phi) + O(\alpha^3), \quad \text{and} \quad K = \frac{\phi \alpha^2}{R_0^2} + O(\alpha^3). \quad (63)$$

That is, up to $O(\alpha^2)$, the mean and Gaussian curvatures of a perturbation of the form (53) are constant.

In a similar way to the above treatment of H and K , both the line element dl , and curvatures q_g and q_n may be expanded in terms of α . However, these quantities also rely on ϵ . To avoid confusion between power series expansions of α and ϵ , we adopt the notation that coefficients are labelled in the following way: in an expansion of some function F , the $O(\alpha^a \epsilon^e)$ term is written as $\alpha^a \epsilon^e F^{(a,e)}$. For example, using this convention, the results of the previous section can be re-labelled. The terms of (45) become

$$dl^{(0,0)} = R_0 d\theta, \quad dl^{(0,1)} = R_0 \sum_n \Re [A_n \exp(i n \theta) d\theta], \quad \text{and} \quad dl^{(0,2)} = \frac{R_0}{2} \sum_n n \Re [i A_n \exp(i n \theta)]^2 d\theta, \quad (64)$$

while the terms of (46) are given by

$$q_g^{(0,0)} = \frac{1}{R_0}, \quad q_g^{(0,1)} = \frac{1}{R_0} \sum_n (n^2 - 1) \Re [\exp(i n \theta)], \quad (65)$$

and

$$q_g^{(0,2)} = \frac{-1}{4 R_0} \sum_n \left\{ |A_n|^2 (3n^2 - 2) + \Re [A_n^2 \exp(2 i n \theta)] \right\}. \quad (66)$$

The full expansions, now in terms of both α and ϵ , take the form

$$dl = dl^{(0,0)} + \epsilon dl^{(0,1)} + \epsilon^2 dl^{(0,2)} + \alpha^2 dl^{(2,0)} + O(\epsilon^3) + O(\alpha^3), \quad (67)$$

and

$$q_g = q_g^{(0,0)} + \epsilon q_g^{(0,1)} + \epsilon^2 q_g^{(0,2)} + \alpha^2 q_g^{(2,0)} + O(\epsilon^3) + O(\alpha^3), \quad (68)$$

where

$$dl^{(1,0)} = 0, \quad \text{and} \quad dl^{(2,0)} = \frac{\psi_{,2}(R_0, \theta)^2}{2 R_0} = \frac{R_0}{8} (\phi - 1)^2 \sin^2(2\theta), \quad (69)$$

and

$$q_g^{(1,0)} = 0, \text{ and } q_g^{(2,0)} = \frac{1}{2R_0^3} [-2\psi_{,2}(R_0, \theta)^2 + \psi_{,22}(R_0, \theta)^2] = \frac{1}{8R_0^2} (1 - \phi)^2 [1 + 3 \cos(4\theta)]. \quad (70)$$

For the normal curvature, we have $q_n = \alpha q_n^{(1,0)} + O(\alpha^3) + O(\epsilon^3)$, where

$$q_n^{(1,0)} = \frac{1}{R_0^2} [\psi_{,22}(R_0, \theta) + R_0 \psi_{,1}(R_0, \theta)] = \frac{1}{2R_0} [1 + \phi + (\phi - 1) \cos(2\theta)]. \quad (71)$$

Substituting the above results into Eq. (40), the necessary integrals can be performed in order to obtain an expansion of \mathcal{H} in terms of both α and ϵ . (Note: the manipulations are quite tedious and we used the commercial software *Mathematica* [25]). If the spontaneous (mean) curvature c_0 is nonzero, then the expansion contains a term

$$\mathcal{H}^{(1,0)} = -2c_0 \kappa \pi R_0 (1 + \phi), \quad (72)$$

In this case, the up / down symmetry of the problem is broken, and *all* perturbations of the form (53), other than a symmetric saddle, are unstable. (A symmetric saddle is given by $c_1 = -c_2$, such that $\phi = -1$ and $H = 0$). By contrast, if the spontaneous curvature is zero, then the energy is of the form

$$\mathcal{H} = \mathcal{H}^{(0,0)} + \epsilon^2 \mathcal{H}^{(0,2)} + \alpha^2 \mathcal{H}^{(2,0)} + O(\epsilon^3) + O(\alpha^3). \quad (73)$$

Here, the line tension τ can once again be fixed for a given R_0 (and material parameters k_g , k_n , q_0 and σ) by imposing $\partial \mathcal{H} / \partial R_0|_{\epsilon=\alpha=0} = 0$. The result is unchanged from (48). In this case $\mathcal{H}^{(0,0)}$ and $\mathcal{H}^{(0,2)}$ can then be read-off from Eq. (49), *i.e.*,

$$\mathcal{H}^{(0,0)} = \pi \left[\frac{k_g}{R_0} (1 - q_0 R_0) - \frac{R_0^2 \sigma}{2} \right], \text{ and } \mathcal{H}^{(0,2)} = \frac{\pi}{2R_0} (n^2 - 1) [k_g (n^2 - 1) - R_0^3 \sigma] \sum_n |A_n|^2. \quad (74)$$

The coefficient of α^2 in (73) is given by

$$\mathcal{H}^{(2,0)} = \pi \left\{ (1 + \phi)^2 2\kappa + (1 - \phi)^2 \frac{3k_g}{8R_0} + \left[(1 + \phi)^2 + 2(1 + \phi^2) \right] \frac{k_n}{8R_0} + \phi \left(\frac{R_0^2 \sigma}{4} + \bar{\kappa} + q_0 k_g \right) \right\}, \quad (75)$$

which can be re-written in the form $\mathcal{H}^{(2,0)} = \pi \phi [\bar{\kappa} - \bar{\kappa}^*(\phi)]$, where

$$\begin{aligned} \bar{\kappa}^* = & -\frac{1}{\phi} (1 + \phi)^2 2\kappa - \frac{1}{\phi} (1 - \phi)^2 \frac{3k_g}{8R_0} - \frac{R_0^2 \sigma}{4} \\ & - \frac{1}{\phi} \left[(1 + \phi)^2 + 2(1 + \phi^2) \right] \frac{k_n}{8R_0} - q_0 k_g, \end{aligned} \quad (76)$$

determines the stability of out-of-plane perturbations. Setting $\phi = -1$ recovers

$$\bar{\kappa}_p^* = \bar{\kappa}^*(-1) = \left(\frac{3}{2R_0} - q_0 \right) k_g + \frac{k_n}{2R_0} - \frac{R_0^2 \sigma}{4}, \quad (77)$$

as shown in the main text.

Higher order contributions

Consider the effect of contributions to the energy of order greater than α^2 . In the expansion of \mathcal{H} , the terms of next lowest order can be calculated, and are at order α^4 . However, to this order, ϵ and α do not de-couple, and we must explicitly set $\epsilon = 0$. [In doing so, we revert to the simple notation that $O(\alpha^n)$ terms in a series expansion of a given function, say F , are written $\alpha^n F^{(n)}$]. In addition, when expanding to $O(\alpha^4)$, the Helfrich Hamiltonian must be modified since Eq. (37) retains only lowest order terms (α^2) by construction. In our framework—*i.e.*, shapes

described by the polar monge field (53)— the requisite higher order terms can be computed, and are given by

$$H^4 = \frac{\alpha^4}{16 R_0^4} (1 + \phi)^4 + O(\alpha^5) \quad (78)$$

$$H^2 K = \frac{\alpha^4}{4 R_0^4} \phi (1 + \phi)^2 + O(\alpha^5), \quad (79)$$

$$K^2 = \frac{\alpha^4}{R_0^4} \phi^2 + O(\alpha^5), \quad (80)$$

$$\Delta H^2 = -\frac{\alpha^4}{2 R_0^4} (1 + \phi)^2 [3(1 + \phi^2) - 2\phi] + O(\alpha^5), \quad (81)$$

$$\Delta K = -\frac{4\alpha^4}{R_0^4} \phi (1 + \phi^2) + O(\alpha^5). \quad (82)$$

When multiplied by their respective moduli and integrated, these terms appear alongside other $O(\alpha^4)$ terms, which arise from the expansions of (37) and (38). Assigning the coefficients λ_i (for $i = 1 \dots 5$) to the contributions (78) to (82), respectively, the resultant fourth order contribution to the energy $\mathcal{H}^{(4,0)}$ is given by

$$\mathcal{H}^{(4,0)} = -\frac{3\pi}{8} \phi (1 + \phi^2) [\bar{\kappa} - \bar{\kappa}_p^\dagger], \quad (83)$$

where

$$\begin{aligned} \bar{\kappa}^\dagger = \frac{8}{3\phi(1+\phi^2)} & \left\{ \kappa \left[-\frac{5}{4} - \frac{3\phi}{2} - \frac{\phi^2}{2} - \frac{2\phi^3}{2} - \frac{5\phi^4}{4} \right] + \frac{k_n}{R_0} \left[-\frac{31}{256} - \frac{5\phi}{64} - \frac{77\phi^2}{128} - \frac{5\phi^3}{64} - \frac{31\phi^4}{256} \right] \right. \\ & + \frac{k_g}{R_0} \left[-\frac{19}{512} - \left(\frac{3q_0 R_0}{8} - \frac{19}{128} \right) \phi - \frac{57\phi^2}{256} - \left(\frac{3q_0 R_0}{8} - \frac{19}{128} \right) \phi^3 - \frac{19\phi^4}{512} \right] \\ & + \sigma R_0^2 \left[-\frac{5}{512} - \frac{3\phi}{128} + \frac{19\phi^2}{768} - \frac{3\phi^3}{128} - \frac{5\phi^4}{512} \right] + \lambda_3 \frac{\phi^2}{R_0^2} - \lambda_5 \frac{4\phi(1+\phi^2)}{R_0^2} \\ & \left. + \frac{(1+\phi)^2}{R_0^2} \left[\lambda_1 \frac{(1+\phi)^2}{16} + \lambda_2 \frac{\phi}{4} - \lambda_4 \left(\frac{3}{2} (1+\phi^2) - \phi \right) \right] \right\}. \end{aligned} \quad (84)$$

Focusing, as before, on saddles with principal curvatures of equal magnitude (so-called “pringles”) we set $\phi = -1$, resulting in

$$\bar{\kappa}_p^\dagger = \frac{19}{24} \frac{k_g}{R_0} + \frac{11}{12} \frac{k_n}{R_0} - k_g q_0 - \frac{5}{72} R_0^2 \sigma - \frac{4}{3} \frac{\lambda_3}{R_0^2} - \frac{32}{3} \frac{\lambda_5}{R_0^2}, \quad (85)$$

where only ΔK and K^2 (*i.e.*, the terms involving Gaussian curvature) contribute from the higher order modifications (78) to (82). The coefficients in the expansion of the energy are now given by $\mathcal{H}^{(2)} = -\pi (\bar{\kappa} - \bar{\kappa}_p^*)$ and $\mathcal{H}^{(4)} = 3\pi (\bar{\kappa} - \bar{\kappa}_p^\dagger)/4$. Due to the introduction of order α^4 contributions, there are now solutions to $\partial\mathcal{H}/\partial\alpha = 0$ at non-zero α , given by

$$\alpha^* = \pm \left(\frac{-\mathcal{H}^{(2)}}{2\mathcal{H}^{(4)}} \right)^{-1/2}. \quad (86)$$

The stability is determined by the coefficient $\mathcal{H}^{(2)}$, via

$$\left. \frac{\partial^2 \mathcal{H}}{\partial \alpha^2} \right|_{\alpha=\alpha^*} = -4 \mathcal{H}^{(2)}, \quad (87)$$

which implies that α^* is only stable if $\bar{\kappa} > \bar{\kappa}_p^*$. In addition, from (86), the expression $-\mathcal{H}^{(2)}/2\mathcal{H}^{(4)}$ must be positive, and we can therefore deduce that $\bar{\kappa} > \max(\bar{\kappa}_p^*, \bar{\kappa}_p^\dagger)$ for stable pringles.

Sorting by modulus of Gaussian Rigidity

Consider a two component nanodiscoid, where the each component has a different modulus of Gaussian rigidity, $\bar{\kappa}_1$ and $\bar{\kappa}_2$. If μ is an area fraction, we write $\bar{\kappa} = \mu \bar{\kappa}_1 + (1 - \mu) \bar{\kappa}_2$ as the average modulus of Gaussian rigidity of the (well mixed) membrane from which the discoids are cut. Relative to the bulk membrane, a pringle on the cusp of formation may contain an additional area fraction ψ of one of the components, resulting in a Gaussian rigidity for the pringle of the form $\bar{\kappa} + \psi \delta \bar{\kappa}$, with $\delta \bar{\kappa} = \bar{\kappa}_1 - \bar{\kappa}_2 > 0$ the difference between the Gaussian rigidities of each component. The membrane Hamiltonian might then include the extra term

$$\mathcal{H}_\psi = \int_S dA \left(\frac{\chi \psi^2}{2} \right), \quad (88)$$

with χ a Flory-like parameter that approaches zero the bulk membrane approaches the demixing transition.

For nanodiscoids subject to a pringle shaped ($\phi = -1$) perturbation,

$$\mathcal{H}_\psi = \frac{\chi \psi^2 \pi R_0^2}{2} \left(1 + \frac{\alpha^2}{4} - \frac{\alpha^4}{48} \right) + O(\alpha^5). \quad (89)$$

The total energy $\mathcal{H} = \mathcal{H}_m + \mathcal{H}_b + \mathcal{H}_\psi$ is then

$$\begin{aligned} \mathcal{H} = \pi \left\{ \left[\frac{k_g}{R_0} (1 - q_0 R_0) - \frac{R_0^2 \sigma}{2} + \frac{\chi \psi^2 R_0^2}{2} \right] + \alpha^2 \left[\frac{\chi \psi^2 R_0^2}{8} - (\bar{\kappa} + \psi \delta \bar{\kappa} - \bar{\kappa}_p^*) \right] \right. \\ \left. + \alpha^4 \left[\frac{3}{4} (\bar{\kappa} + \psi \delta \bar{\kappa} - \bar{\kappa}_p^\dagger) - \frac{\chi \psi^2 R_0^2}{96} \right] \right\} + O(\alpha^5). \end{aligned} \quad (90)$$

The additional area fraction ψ of the pringle's surface that is occupied by the component $\bar{\kappa}_1$ is found by imposing $\partial \mathcal{H} / \partial \psi = 0$, which implies

$$\psi^2 = \frac{(\delta \bar{\kappa})^2}{\chi^2 R_0^4} \alpha^4 + O(\alpha^5). \quad (91)$$

Substituting into (89) gives

$$H_\psi = \frac{\pi (\delta \bar{\kappa})^2}{2 \chi R_0^2} + O(\alpha^5), \quad (92)$$

and hence

$$\mathcal{H} = \pi \left\{ \left[\frac{k_g}{R_0} (1 - q_0 R_0) - \frac{R_0^2 \sigma}{2} \right] - \alpha^2 (\bar{\kappa} - \bar{\kappa}_p^*) + \frac{3\alpha^4}{4} \left[\bar{\kappa} - \left(\bar{\kappa}_p^\dagger - \frac{2(\delta \bar{\kappa})^2}{3 \chi R_0^2} \right) \right] \right\} + O(\alpha^5). \quad (93)$$

Writing

$$\bar{\kappa}_\chi^\dagger = \bar{\kappa}_p^\dagger - \frac{2(\delta \bar{\kappa})^2}{3 \chi R_0^2}, \quad (94)$$

implies non-zero stable solutions α^* , and hence principal curvatures of magnitude

$$|c_1| = \frac{1}{R_0} \left[\frac{2(\bar{\kappa} - \bar{\kappa}_p^*)}{3(\bar{\kappa} - \bar{\kappa}_\chi^\dagger)} \right]^{1/2}, \quad (95)$$

for average Gaussian curvatures $\bar{\kappa} > \max(\bar{\kappa}_p^*, \bar{\kappa}_\chi^\dagger)$.

IMAGE ANALYSIS

Two cryo Electron Microscopy images were analysed, one is shown in Fig. 3 of the main manuscript, and the other is displayed in Fig. 5. Images were analysed according to the following protocol. In order to remove unwanted noise,

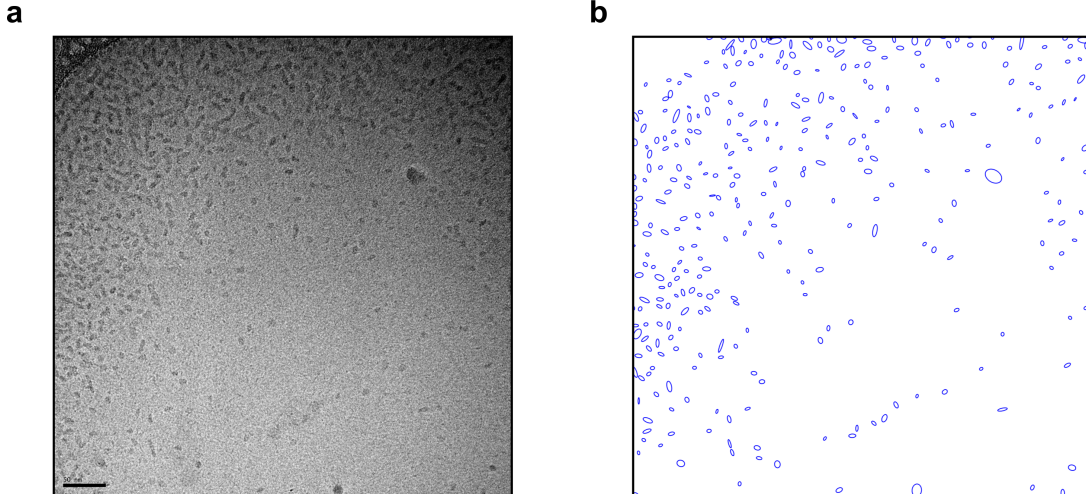


FIG. 5. (Color online) Cryo Electron Microscopy image (a) and associated image analysis (b) of Styrene Maleic Acid stabilised nanodiscoids, prepared according to [4] (scale bar = 50 nm).

images were pre-processed using the free application ImageJ. After conversion to an 8-bit single channel image, a small Gaussian blur was applied (10 pixel variance) followed by a low pass filter, set to remove structures below 15 pixels in size (1 pixel = 0.131 nm). The identification and fitting of shapes was carried out using the freely available OpenCV library of Python functions. First, the pre-processed image was thresholded, after which discoid contours were extracted. Ellipses were then fitted to the discoid contours using an in-built least-squares procedure. We remark that the protocol relies on edge-detection via contrast, and hence is not well suited to differentiating between overlapping SMALPs or identifying those that are out of the focal plane.

In total, the analysis identified 414 SMALPs across both images. The average length of the ellipse semi-major axes was 3.48 nm, with a variance of 1.68 nm^2 .